IEEE Access
Multidisciplinary | Rapid Review | Open Access Journal

Received 28 April 2025, accepted 10 May 2025, date of publication 14 May 2025, date of current version 23 May 2025.

Digital Object Identifier 10.1109/ACCESS.2025.3569979

RESEARCH ARTICLE

Experimental Evaluation of a 2DOF Controller for a Novel Multi-Temperature Transport System

MAXIMILIAN LÖSCH, STEFAN JAKUBEK, AND MARTIN KOZEK
Institute of Mechanics and Mechatronics, TU Wien, 1060 Vienna, Austria

Corresponding author: Maximilian Lösch (maximilian.loesch@tuwien.ac.at)

This work was supported in part by Austrian Research Promotion Agency (Forschungsförderungsgesellschaft) through the project ZETA under Grant 891917, and in part by TU Wien Bibliothek through the Open Access Funding Program.

ABSTRACT Multi-temperature transport systems offer a significant opportunity to improve supply chain efficiency by enabling the simultaneous transport of goods with diverse temperature requirements. However, these systems present critical environmental challenges due to high energy consumption, refrigerant leakage, and the significant amount of goods being damaged or lost due to inadequate temperature control. To address these issues, this study proposes a novel indirect cascade multi-temperature transport system with two temperature-controlled compartments. The design features a compact, well-sealed refrigeration system with reduced refrigerant charge and utilizes the natural refrigerant propane. A nonlinear control strategy based on feedback linearization is introduced to decouple system dynamics and precisely regulate compartment temperatures. Specifically, a two-degree-of-freedom (2DOF) controller, consisting of a feedforward trajectory planning algorithm and a feedback controller, is implemented. Additionally, an optimization-based input transformation allows prioritization of specific compartments when actuator limitations prevent accurate tracking of all compartment temperatures. The control approach was experimentally evaluated on a test bed and compared with a conventional proportional-integral (PI) controller. Across the conducted experiments, the proposed 2DOF control law reduced temperature deviations during normal operation by 40% to 77%, clearly highlighting its quantitative superiority over the conventional approach.

INDEX TERMS Feedback linearization, nonlinear control systems, refrigerated transport, temperature control.

I. INTRODUCTION

Refrigerated transport systems pose a significant environmental challenge, with approximately 15% of global fossil fuel energy consumed in refrigerated food transport [1] and 10% of worldwide greenhouse gas emissions attributed to vapor compression refrigeration systems [2]. A considerable share of these emissions stems from refrigerant leakage in vapor compression cycles, with refrigerated trucks losing between 10% and 37% of their refrigerant charge annually [3]. This leakage has two major environmental consequences: the direct release of greenhouse gases, as commonly used refrigerants exhibit a global warming potential (GWP) over 1000 times that of CO_2, and the indirect increase in emissions due to reduced refrigeration system efficiency caused by suboptimal refrigerant charge [4], [5]. The environmental impact is particularly pronounced in multi-temperature systems with multiple compartments, which require large refrigerant charges and incorporate more complex, distributed refrigerant cycles [6]. Moreover, these systems face challenges in temperature control [7], often resulting in variations of the compartment temperatures, which can damage or spoil transported goods, thereby compounding their environmental impact.

To address these challenges, this work proposes an indirect cascade refrigeration system that utilizes secondary loops with two temperature-controlled compartments. Compared to conventional multi-temperature transport systems, the proposed design reduces the required refrigerant charge, is less prone to refrigerant leakage, and employs the natural refrigerant propane with a low GWP, thus significantly reducing the system's environmental impact. For temperature

The associate editor coordinating the review of this manuscript and approving it for publication was Zheng Chen.

© 2025 The Authors. This work is licensed under a Creative Commons Attribution 4.0 License.
For more information, see https://creativecommons.org/licenses/by/4.0/

regulation of the two compartments, a two-degree-of-freedom (2DOF) controller based on feedback linearization is proposed, effectively decoupling the dynamics of the compartment temperatures. The proposed control concept was experimentally evaluated on a test bed of the proposed refrigeration system and compared to a proportional-integral (PI) controller, a widely adopted control method in the cold-chain industry.

Traditionally, goods with different temperature requirements were transported separately. However, recent advancements have led to the development of multi-temperature transport systems, which feature multiple compartments that can be individually held at different temperature levels. This enables the simultaneous transport of goods with diverse temperature needs - such as frozen, fresh, and ambient products in food logistics [8]. These systems offer significant advantages in temperature-controlled logistics, including enhanced flexibility, fewer stops, and reduced mileage. Studies [9], [10], [11] indicate that fleet costs can be reduced by 6%-30% when employing multi-compartment vehicles, compared to fleets relying only on single-compartment vehicles. Despite these clear benefits, multi-temperature refrigeration systems remain relatively uncommon [12].

Hydrofluorocarbon (HFC) refrigerants are the most commonly used refrigerants in the cold chain industry [13], [14]. However, due to their substantial environmental impact - particularly their high GWP and contribution to ozone depletion - many countries have committed to phasing them out until 2050 [15]. Consequently, considerable efforts are being directed toward identifying alternative refrigerants that offer comparable efficiency and capacity while being more environmentally sustainable. Among the most promising candidates for temperature-controlled transport are the natural refrigerants propane and CO_2 [16]. While propane exhibits more favorable thermodynamic and transport properties than CO_2, it poses an inherent flammability risk [17]. Both refrigerants are already in commercial use, and studies have shown that systems utilizing CO_2 [18] or propane [19], [20] can achieve similar or even better energy efficiencies than conventional HFC-based systems. Therefore, these alternative refrigerants not only have the potential to reduce direct emissions of the refrigerant significantly but also contribute to lowering indirect emissions by improving the efficiency of refrigeration systems.

In multi-temperature systems, a simple vapor compression cycle is insufficient due to its limitation of extracting heat from only a single temperature level, owing to its single evaporator configuration. Consequently, more advanced systems are required, and various multi-temperature systems have been developed, as summarized in [21]. One of the most established approaches is the cascade cycle. Cascade systems consist of multiple cooling cycles connected in series, enabling heat extraction from different temperature levels. They offer several advantages over single cycles, including a broader temperature range, higher capacity, and an improved coefficient of performance [22], [23]. In [24], several cascade cycles for multi-temperature refrigeration are compared regarding energy, exergy, and economic performance. They proposed a system with a single high-temperature cycle connected to two low-temperature cycles, which demonstrated superior performance in the aforementioned aspects compared to traditional systems.

In multi-temperature transport systems, direct expansion (DX) refrigeration technology is predominantly employed [25]. In DX systems, the evaporators are located directly inside the compartments, resulting in large refrigerant charges and leak-prone distribution pipes leading to the distributed evaporators. The adoption of propane as a refrigerant heightens safety concerns, as leaks inside the compartments pose significant safety hazards. These risks can be mitigated by employing indirect expansion (IDX) technologies, where secondary loops act as an intermediary between the primary cooling cycle and the interior of the compartments [26]. Typically, a non-hazardous fluid, such as a water-glycol mixture, is used in the secondary loop to serve as a heat transfer medium [27]. Consequently, the primary cooling loop can be designed to be compact, well-sealed, and located outside the compartments, significantly reducing safety risks, refrigerant charge, and leakage potential. A comparative analysis presented in [28] evaluated a multi-temperature refrigeration system with IDX, despite only equipping one of the two compartments with a secondary loop, against one with DX and found that while the refrigerant charge could be reduced on average by 58.5%, the energy consumption increased by 2.5% to 17.1% due to the lower evaporation temperature with IDX systems. Nevertheless, the study concluded that the overall environmental impact was reduced by 30% with the IDX system, based on the metrics used. Similar findings have been reported in [29] and [30]. However, in literature on indirect cascade multi-temperature refrigeration systems, secondary loops have mainly been applied to a single compartment rather than all, indicating a research gap in exploring the full benefits of IDX systems.

Accurate temperature control is critical for maintaining the quality and safety of goods within the cold chain, and even minor temperature deviations can lead to the loss or damage of goods [31]. However, achieving precise temperature regulation in refrigerated transport systems is especially difficult for multi-temperature systems [7], as they consist of multiple compartments with strongly coupled dynamics. These coupled dynamics are particularly concerning, as they can cause significant deviations and oscillations of the compartment temperatures during closed-loop operation. Despite these challenges, the industry predominantly relies on relatively simple controllers, such as proportional–integral–derivative (PID) controllers, which research has shown are not well-suited for fullfilling the complex requirements of refrigerated transport system [32].

In [33], a model predictive controller (MPC) is proposed for regulating a DX multi-evaporator vapor compression

system. Based on a linearized model, this approach satisfied requirements for setpoint regulation and energy efficiency but did not explicitly address the coupled dynamics, leading to temperature oscillations around the setpoint. Another study [34] analyzed the coupling effects of a similar DX multi-evaporator vapor compression system and proposed a decoupling MPC to control the cooling capacity of each evaporator. However, the work lacks experimental validation and focuses only on the refrigeration cycle, neglecting the essential interaction with the compartments. While the aforementioned studies relied on linear models of the vapor compression cycle, the dynamics of vapor compression systems are inherently nonlinear [35]. In [36] and [37], nonlinear decoupling control strategies based on feedback linearization are proposed for indoor climate control systems in buildings, featuring a single cooling cycle and variable airflow distribution to different temperature zones. Simulation results demonstrate the superiority of this approach in disturbance rejection and decoupling compared to a conventional PI controller. However, their system architecture with a single cooling cycle differs significantly from the multi-temperature transport system discussed here. Furthermore, machine learning and data-driven control strategies have gained significant traction in recent years, for example in the control of power systems [38]. While these methods often deliver good control performance - even though they are mostly model-free - and can approximate decoupling by learning the system dynamics, they typically do not address decoupling explicitly. As a result, residual coupling effects may persist, potentially limiting their effectiveness in highly coupled systems such as the one discussed here.

Existing literature on cascade refrigeration systems [39], [40] primarily focuses on energy efficiency and exclusively considers a single controlled temperature level. Research on decoupling control methods for cascade refrigeration systems is lacking, although such systems could significantly benefit from these methods due to the highly coupled dynamics intrinsically arising from their architecture. This work contributes not only by addressing this gap theoretically, by proposing a decoupling control concept for such systems, but also by demonstrating its practical application on a real-world test bed. To summarize, the novel contributions that set this work apart from existing literature include:

- Novel indirect cascade refrigeration system with a leak-proof design and minimal refrigerant charge.
- Nonlinear decoupling control concept for precise temperature regulation across multiple compartments in a cascaded refrigeration system.

The remainder of this work is structured as follows: The architecture of the multi-temperature transport system is described in Section II. Section III introduces the control scheme, covering system modeling, feedback linearization, the 2DOF controller, and the PI controller used for comparison. In Section IV, the experimental evaluation of the refrigeration system and its control scheme is presented. The work concludes with a discussion in Section V and a conclusion in Section VI.

In this paper, temperature values in Kelvin are denoted by the symbol T, while those in degrees Celsius are represented by ϑ, with the conversion between Kelvin and Celsius given by $T = \vartheta + 273.15$.

II. MULTI-TEMPERATURE TRANSPORT SYSTEM

The multi-temperature transport system under consideration is illustrated in Fig. 1, where the measured temperatures are denoted by T, heat flows by $\dot{Q}$, and the compressor speeds of the cooling cycles by $n_{\mathrm{cpr},1}$ and $n_{\mathrm{cpr},2}$. The system comprises two compartments: the medium temperature (MT) compartment and the low temperature (LT) compartment, with the air temperatures within these compartments represented by the variables $T_{\mathrm{c}}^{\mathrm{mt}}$ and $T_{\mathrm{c}}^{\mathrm{lt}}$, respectively. The system employs an indirect cascade refrigeration system, consisting of two cooling cycles and two glycol loops ($T_{\mathrm{g}}^{\mathrm{mt}}$, $T_{\mathrm{g}}^{\mathrm{lt}}$), which serve as secondary loops to the cooling cycles. The cooling cycles are vapor compression cycles that use the natural refrigerant propane. These cycles are driven by a compressor with the rotational speed $n_{\mathrm{cpr},i},\ i \in \{1, 2\}$, removing a heat flow $\dot{Q}_{\mathrm{ev},i},\ i \in \{1, 2\}$ from the evaporator side. On the condenser side of cooling cycle 2, the heat flow $\dot{Q}_{\mathrm{co},2}$ is transferred to the MT glycol loop, whereas the condenser of cooling cycle 1 is air-cooled by ambient air with the temperature T_{a}. Inside the compartments, heat exchangers facilitate the heat flows $\dot{Q}_{\mathrm{he}}^{\mathrm{mt}}$ and $\dot{Q}_{\mathrm{he}}^{\mathrm{lt}}$ between the glycol loops and their respective compartments. Exogenous disturbances, such as solar radiation, door openings, and heat from transported goods, also influence the compartment temperatures, represented in this system by the variables $\dot{Q}_{\mathrm{d}}^{j},\ j \in \{\mathrm{mt}, \mathrm{lt}\}$.

The fans mounted to the heat exchangers inside the compartments, the one mounted to the condenser of cooling cycle 1, and the pumps of the MT and LT glycol loop all operate at constant speed. Therefore, they are not considered as variables in this work.

Due to the design of the proposed refrigeration system, the MT compartment can be heated and cooled because its glycol loop is connected to both the condenser of cooling cycle 2 and the evaporator of cooling cycle 1. In contrast, the LT compartment can only be cooled, but the cascade architecture allows it to reach lower temperatures than the MT compartment.

The system architecture enables a simple and compact implementation of the two cooling cycles, which also facilitates their hermetic sealing. As a result, the multi-temperature refrigeration system requires only a minimal refrigerant charge, and the risk of refrigerant leakage is significantly reduced.

The dynamics of both compartment temperatures are coupled due to the connection between the two compartments via the glycol loops and cooling cycle 2. As a result, temperature changes in one compartment influence the other,

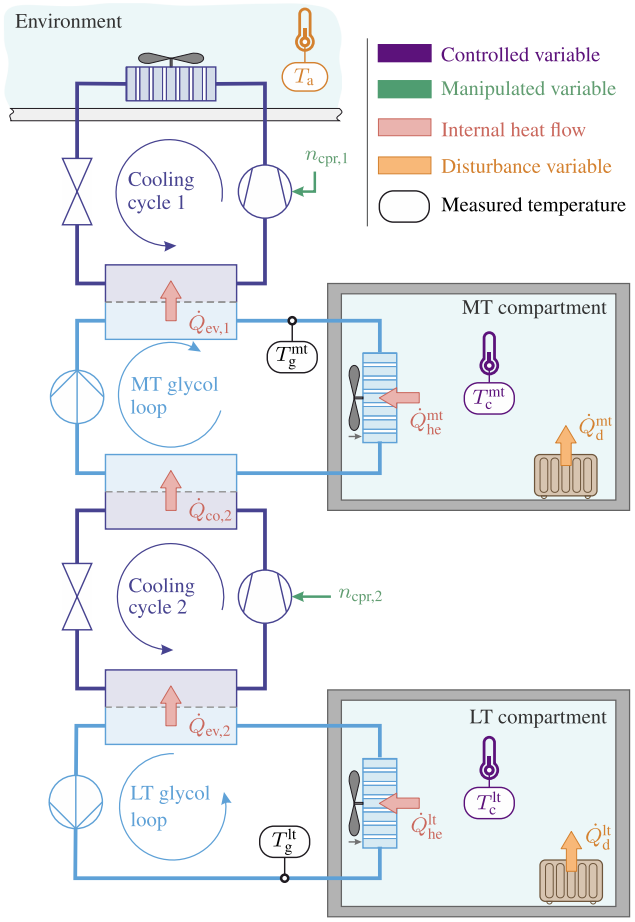

FIGURE 1. Schematic illustration of the indirect cascade refrigeration system with two temperature-controlled compartments. The system utilizes two vapor compression cooling cycles connected by glycol loops. Key variables, including measured temperatures (T), heat flows ($\dot{Q}$), and the variable compressor speeds ($n_{cpr,1}$, $n_{cpr,2}$), are highlighted.

and both compressor speeds, which are later used for control, impact the temperatures of both compartments. These coupled dynamics require a dedicated control algorithm to ensure precise temperature regulation in both compartments.

III. CONTROL SCHEME

The primary control objective is to accurately track reference temperature values for each compartment. Additionally, the temperature dynamics of each compartment should be decoupled to prevent disturbances in one compartment or changes in its reference temperature from affecting the other. To achieve this, a 2DOF controller was selected, employing feedback linearization applied to a nonlinear model of the multi-temperature transport system. The following sections detail the derivation of this control law and introduce a baseline control scheme without decoupling, which acts as a benchmark for evaluating the 2DOF controller's performance.

A. MODEL DESCRIPTION

This section presents a control-oriented model of the system, which serves as the basis for the decoupling control scheme. Hence, it is essential that the model accurately captures all key dynamics relevant to control while remaining as simple as possible to minimize computational effort. The mathematical formulation follows a lumped-parameter approach, with model parameters estimated from experimental data, resulting in a grey-box modeling framework. Following this common approach [41], [42], each compartment is represented by a single lumped temperature. The dynamic model of each compartment is formulated using an energy balance equation in continuous time t, accounting for inflowing and outflowing heat flows as well as heat losses through the walls:

$$C_c^{mt}\frac{dT_c^{mt}(t)}{dt} = -\dot{Q}_{he}^{mt}(t) + \dot{Q}_d^{mt}(t) + K_w^{mt}[T_a(t) - T_c^{mt}(t)] \tag{1}$$

$$C_c^{lt}\frac{dT_c^{lt}(t)}{dt} = -\dot{Q}_{he}^{lt}(t) + \dot{Q}_d^{lt}(t) + K_w^{lt}[T_a(t) - T_c^{lt}(t)], \tag{2}$$

where the heat capacity of the air inside the compartments, C_c^{mt} and C_c^{lt}, and the thermal conductance of the compartment walls, K_w^{mt} and K_w^{lt}, are constant parameters. Similarly, the two glycol loops are modeled using lumped temperatures, with their dynamics given by:

$$C_g^{mt}\frac{dT_g^{mt}(t)}{dt} = -\dot{Q}_{ev,1}(t) + \dot{Q}_{co,2}(t) + \dot{Q}_{he}^{mt}(t) \tag{3}$$

$$C_g^{lt}\frac{dT_g^{lt}(t)}{dt} = -\dot{Q}_{ev,2}(t) + \dot{Q}_{he}^{lt}(t) \tag{4}$$

with C_g^{mt} and C_g^{lt} representing the heat capacity of the MT and LT glycol loop, respectively. The assumption of lumped temperatures relies on minimal temperature variations within the compartments and glycol loops. This assumption remains valid when sufficient mixing is ensured by heat exchanger fans or pumps within the glycol loops.

For modeling the heat exchangers within the compartments, the effectiveness-NTU method is used [43]. Assuming constant mass flow rates for both air and glycol due to the continuous operation of the fans and pumps, the heat transfer between the glycol loop and the air inside the compartment is given by:

$$\dot{Q}_{he}^{j}(t) = K_c^{j}[T_c^{j}(t) - T_g^{j}(t)], \quad j \in \{\text{mt}, \text{lt}\} \tag{5}$$

with the heat transfer coefficients K_c^{mt} and K_c^{lt}.

Each of the two cooling cycles is modeled by a nonlinear static relation for the heat flows on the evaporator and condenser side. Since the most influential variables in the cooling cycle are the compressor speed and the evaporator and condenser temperatures, the heat flows are modeled as follows:

$$\dot{Q}_{ev,1}(t) = [\alpha_{1,1}T_a(t) + \alpha_{2,1}T_g^{mt}(t) + \alpha_{3,1}]n_{cpr,1}(t) \tag{6}$$

$$\dot{Q}_{ev,2}(t) = [\alpha_{1,2}T_g^{mt}(t) + \alpha_{2,2}T_g^{lt}(t) + \alpha_{3,2}]n_{cpr,2}(t) \tag{7}$$

$$\dot{Q}_{co,2}(t) = [\beta_{1,2}T_g^{mt}(t) + \beta_{2,2}T_g^{lt}(t) + \beta_{3,2}]n_{cpr,2}(t) \tag{8}$$

with the parameters $\alpha_{1,1}, \alpha_{2,1}, \alpha_{3,1}, \alpha_{1,2}, \alpha_{2,2}, \alpha_{3,2}, \beta_{1,2}, \beta_{2,2}$, and $\beta_{3,2}$. The dynamic behavior of the refrigeration cycle is neglected, following a common approach in control-oriented modeling of refrigerated transport systems [42], [44]. This simplification is justified because the internal processes within the cycle are significantly faster than the overall system dynamics due to the large heat capacities of the glycol loops and compartments.

The equations above are assembled into the general form of a nonlinear input-affine state-space system to provide a concise description of the model according to

$$\dot{\boldsymbol{x}}(t, \boldsymbol{\theta}) = \mathrm{f}(\boldsymbol{x}, \boldsymbol{d}, \boldsymbol{\theta}) + \mathrm{g}(\boldsymbol{x}, \boldsymbol{d}, \boldsymbol{\theta})\boldsymbol{u}(t) \tag{9}$$

with the vector fields f and g, the state vector $\boldsymbol{x}$ defined by

$$\boldsymbol{x}(t) = \left[T_{\mathrm{g}}^{\mathrm{mt}}, T_{\mathrm{g}}^{\mathrm{lt}}, T_{\mathrm{c}}^{\mathrm{mt}}, T_{\mathrm{c}}^{\mathrm{lt}}\right]^{\mathrm{T}}, \tag{10}$$

the input vector of the manipulated variables $\boldsymbol{u}$

$$\boldsymbol{u}(t) = \left[n_{\mathrm{cpr},1}, n_{\mathrm{cpr},2}\right]^{\mathrm{T}}, \tag{11}$$

the disturbances $\boldsymbol{d}$ given by

$$\boldsymbol{d}(t) = \left[T_{\mathrm{a}}, \dot{Q}_{\mathrm{d}}^{\mathrm{mt}}, \dot{Q}_{\mathrm{d}}^{\mathrm{lt}}\right]^{\mathrm{T}}, \tag{12}$$

and the vector of the model parameters $\boldsymbol{\theta}$ according to:

$$\begin{aligned}\boldsymbol{\theta} = [&C_{\mathrm{c}}^{\mathrm{mt}}, C_{\mathrm{c}}^{\mathrm{lt}}, C_{\mathrm{g}}^{\mathrm{mt}}, C_{\mathrm{g}}^{\mathrm{lt}}, K_{\mathrm{c}}^{\mathrm{mt}}, K_{\mathrm{c}}^{\mathrm{lt}}, K_{\mathrm{w}}^{\mathrm{mt}}, K_{\mathrm{w}}^{\mathrm{lt}},\\ &\ldots \alpha_{1,1}, \alpha_{2,1}, \alpha_{3,1}, \alpha_{1,2}, \alpha_{2,2}, \alpha_{3,2}, \beta_{1,2}, \beta_{2,2}, \beta_{3,2}]^{\mathrm{T}}.\end{aligned} \tag{13}$$

The model parameters are estimated using experimentally obtained measurement data recorded at discrete time instances $t_k, k \in \{1, \ldots, n_k\}$. The estimation method minimizes the quadratic model error $\Delta\boldsymbol{x}$, defined as

$$\Delta\boldsymbol{x}(t_k, \boldsymbol{\theta}) = \boldsymbol{x}(t_k, \boldsymbol{\theta}) - \boldsymbol{x}_{\mathrm{meas}}(t_k), \tag{14}$$

where $\boldsymbol{x}_{\mathrm{meas}}$ represents the measured state variables. The model states $\boldsymbol{x}$ over time are determined by solving the nonlinear state-space model using the inputs and disturbances from the measurement dataset. The parameter vector is then estimated by solving

$$\boldsymbol{\theta} = \arg\min_{\boldsymbol{\theta}} \frac{1}{n_k} \sum_{k=1}^{n_k} \Delta\boldsymbol{x}(t_k, \boldsymbol{\theta})^{\mathrm{T}} \Delta\boldsymbol{x}(t_k, \boldsymbol{\theta}). \tag{15}$$

Section IV-B presents the results of the parameter estimation and the corresponding model.

B. FEEDBACK LINEARIZATION

In this section, the method of feedback linearization is applied to the nonlinear model derived in the previous section. This transformation not only provides an equivalent linear system representation by transforming the system's states and control variables but also decouples the dynamics of the model's outputs. For brevity, the method is applied directly to the considered system, but interested readers can refer to [45] and [46] for a more detailed and general explanation of the method.

Recapitulating the state-space model (9) and incorporating the output equations $\mathrm{h}_1(x)$ and $\mathrm{h}_2(x)$, we obtain the following formulation

$$\begin{aligned}\dot{\boldsymbol{x}} &= \mathrm{f}(\boldsymbol{x}, \boldsymbol{d}) + \mathrm{g}(\boldsymbol{x}, \boldsymbol{d})\boldsymbol{u}\\ \boldsymbol{y} &= \begin{bmatrix} y_1 \\ y_2 \end{bmatrix} = \begin{bmatrix} T_{\mathrm{c}}^{\mathrm{mt}} \\ T_{\mathrm{c}}^{\mathrm{lt}} \end{bmatrix} = \begin{bmatrix} \mathrm{h}_1(\boldsymbol{x}) \\ \mathrm{h}_2(\boldsymbol{x}) \end{bmatrix},\end{aligned} \tag{16}$$

where the output vector $\boldsymbol{y}$ summarizes the compartment temperatures that should be controlled.

Using the notation of Lie derivatives, the first time derivative of the i-th output is given by

$$\begin{aligned}\dot{y}_i &= \frac{\partial \mathrm{h}_i(\boldsymbol{x})}{\partial \boldsymbol{x}}[\mathrm{f}(\boldsymbol{x}, \boldsymbol{d}) + \mathrm{g}(\boldsymbol{x}, \boldsymbol{d})\boldsymbol{u}]\\ &= L_{\mathrm{f}}\mathrm{h}_i(\boldsymbol{x}, \boldsymbol{d}) + L_{\mathrm{g}}\mathrm{h}_i(\boldsymbol{x}, \boldsymbol{d})\boldsymbol{u}, \quad i \in \{1, 2\}.\end{aligned} \tag{17}$$

Since $L_{\mathrm{g}}\mathrm{h}_i(\boldsymbol{x}, \boldsymbol{d}) = 0$ for all $i \in \{1, 2\}$, the first time derivative of both outputs is independent of the inputs $\boldsymbol{u}$. In the absence of additional information about the disturbances $\boldsymbol{d}$, we assume $\dot{\boldsymbol{d}}(t) = 0$, leading to the second time derivative of the i-th output according to:

$$\ddot{y}_i = L_{\mathrm{f}}^2\mathrm{h}_i(\boldsymbol{x}, \boldsymbol{d}) + L_{\mathrm{g}}L_{\mathrm{f}}\mathrm{h}_i(\boldsymbol{x}, \boldsymbol{d})\boldsymbol{u}, \quad i \in \{1, 2\}. \tag{18}$$

Since $L_{\mathrm{g}}L_{\mathrm{f}}\mathrm{h}_i(\boldsymbol{x}, \boldsymbol{d})$ is nonzero for both outputs, the input-output relation is expressed in vector form as

$$\begin{aligned}\ddot{\boldsymbol{y}} &= \begin{bmatrix} \ddot{y}_1 \\ \ddot{y}_2 \end{bmatrix} = \begin{bmatrix} L_{\mathrm{f}}^2\mathrm{h}_1(\boldsymbol{x}, \boldsymbol{d}) \\ L_{\mathrm{f}}^2\mathrm{h}_2(\boldsymbol{x}, \boldsymbol{d}) \end{bmatrix} + \begin{bmatrix} L_{\mathrm{g}}L_{\mathrm{f}}\mathrm{h}_1(\boldsymbol{x}, \boldsymbol{d}) \\ L_{\mathrm{g}}L_{\mathrm{f}}\mathrm{h}_2(\boldsymbol{x}, \boldsymbol{d}) \end{bmatrix}\boldsymbol{u}\\ &= \boldsymbol{l}(\boldsymbol{x}, \boldsymbol{d}) + \boldsymbol{J}(\boldsymbol{x}, \boldsymbol{d})\boldsymbol{u}\end{aligned} \tag{19}$$

with the vector field $\boldsymbol{l}$ and the coupling matrix $\boldsymbol{J}$. Assuming that $\boldsymbol{J}$ is nonsingular, as is verified in Appendix C, and given that the system order of the input-output dynamics (19) matches the order of the original system (16), the system exhibits full relative degree. Consequently, all dynamics of the original system are observable through the input-output dynamics, allowing the system to be expressed in Brunovsky form:

$$\dot{\boldsymbol{z}} = \boldsymbol{A}\boldsymbol{z} + \boldsymbol{B}\boldsymbol{v} \tag{20}$$

with system matrix $\boldsymbol{A}$, the input matrix $\boldsymbol{B}$, the state transformation $\phi(\boldsymbol{x}, \boldsymbol{d})$ defined by

$$\boldsymbol{z} = \begin{bmatrix} y_1 \\ \dot{y}_1 \\ y_2 \\ \dot{y}_2 \end{bmatrix} = \begin{bmatrix} h_1(\boldsymbol{x}) \\ L_{\mathrm{f}}\mathrm{h}_1(\boldsymbol{x}, \boldsymbol{d}) \\ h_2(\boldsymbol{x}) \\ L_f h_2(\boldsymbol{x}, \boldsymbol{d}) \end{bmatrix} = \phi(\boldsymbol{x}, \boldsymbol{d}) \tag{21}$$

and input transformation for the virtual inputs v given by

$$\boldsymbol{v} = \boldsymbol{l}(\boldsymbol{x}, \boldsymbol{d}) + \boldsymbol{J}(\boldsymbol{x}, \boldsymbol{d})\boldsymbol{u}. \tag{22}$$

It is important to note that both transformations can be inverted. The inverse of transformation (21) exists and is denoted as $\phi^{-1}(\boldsymbol{x}, \boldsymbol{d})$, and since $\boldsymbol{J}(\boldsymbol{x}, \boldsymbol{d})$ is assumed to be nonsingular, the inputs $\boldsymbol{u}$ can be calculated from the virtual inputs $\boldsymbol{v}$ as follows:

$$\boldsymbol{u} = \boldsymbol{J}^{-1}(\boldsymbol{x}, \boldsymbol{d})[\boldsymbol{v} - \boldsymbol{l}(\boldsymbol{x}, \boldsymbol{d})]. \tag{23}$$

This transformation results in a linear and fully decoupled system with respect to the virtual inputs $\boldsymbol{v}$, where each virtual input independently controls one output through a chain of integrators. This property becomes evident when applying the Laplace transformation to (20), yielding the transfer function matrix $G(s)$:

$$G(s) = \frac{Y(s)}{V(s)} = \begin{bmatrix} 1/s^2 & 0 \\ 0 & 1/s^2 \end{bmatrix}, \tag{24}$$

where s is the Laplace variable. As a result, the virtual inputs $\boldsymbol{v}$ enable independent control of the two outputs, ensuring that each input affects only its corresponding output without influencing the other.

The following section presents a decoupling controller that leverages the decoupled linear system derived here.

C. 2DOF CONTROLLER

In this section, we introduce a 2DOF controller, as illustrated in Fig. 2. The control law comprises a feedforward trajectory planning, a feedback controller, and an input transformation from the virtual inputs $\boldsymbol{v}$ to the inputs $\boldsymbol{u}$.

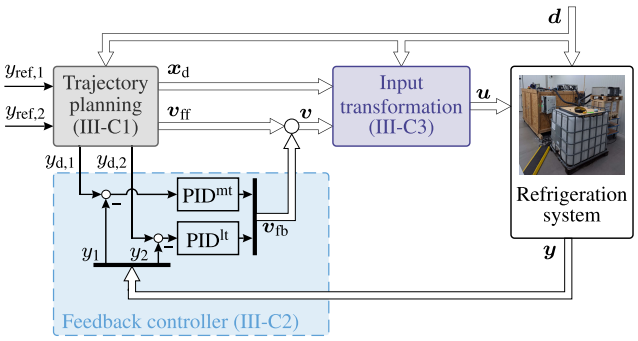

FIGURE 2. Visualization depicting the control architecture of the 2DOF controller. Section numbers providing detailed information are given in brackets.

1) TRAJECTORY PLANNING

The temperatures inside the compartments should follow a predefined trajectory $\boldsymbol{y}_\mathrm{d}$, such as during the initial cooldown or when new target temperatures are set. In general, any sufficiently smooth trajectory $\boldsymbol{y}_\mathrm{d}$ can be chosen here. For the system considered, both output trajectories must be at least once continuously differentiable to ensure a realizable state trajectory $\boldsymbol{x}_\mathrm{d}$, which is obtained by applying the inverse state transformation given in (21):

$$\boldsymbol{x}_\mathrm{d}(t) = \phi^{-1}(\boldsymbol{z}_d, \boldsymbol{d}), \quad \boldsymbol{z}_\mathrm{d}(t) = [y_{\mathrm{d},1}, \dot{y}_{\mathrm{d},1}, y_{\mathrm{d},2}, \dot{y}_{\mathrm{d},2}]^\mathrm{T}. \tag{25}$$

The virtual inputs $\boldsymbol{v}_\mathrm{ff}$ required to realize this trajectory are given by

$$\boldsymbol{v}_\mathrm{ff}(t) = [\ddot{y}_{\mathrm{d},1}, \ddot{y}_{\mathrm{d},2}]^\mathrm{T}, \tag{26}$$

which may be discontinuous but finite. In this work, the desired trajectories are constructed by applying a second-order filter to the desired temperature values of the compartments $\boldsymbol{y}_\mathrm{ref} = [y_{\mathrm{ref},1}, y_{\mathrm{ref},2}]^\mathrm{T}$:

$$\tau_i^2 \ddot{y}_{\mathrm{d},i}(t) + 2\lambda_i \tau_i \dot{y}_{\mathrm{d},i}(t) + y_{\mathrm{d},i}(t) = y_{\mathrm{ref,i}}(t), \quad i \in \{1, 2\} \tag{27}$$

with the time constant τ_i and the damping factor λ_i. By utilizing the inverse input transformation (23) and applying the feedforward control law (26), the desired trajectory will be precisely tracked in the absence of model errors, unknown disturbances, and deviations from the initial conditions. Moreover, even in the presence of sufficiently small model uncertainties, unknown disturbances, or deviations from the initial conditions, the system will remain in the vicinity of the desired trajectory, as proven in [47]. To eliminate these tracking errors, a feedback controller is added to the control law.

2) FEEDBACK CONTROLLER

The tracking errors, e_1 and e_2, of the two compartment temperatures are defined as the difference between the desired temperature trajectory and the actual temperature:

$$e_i(t) = y_{\mathrm{d},i}(t) - y_i(t), \quad i \in \{1, 2\}. \tag{28}$$

To correct for these errors, we employ a PID controller [48] for each output, prescribing the feedback action $\boldsymbol{v}_\mathrm{fb} = [v_{\mathrm{fb},1}, v_{\mathrm{fb},2}]^\mathrm{T}$, given by

$$v_{\mathrm{fb},i}(t) = K_{\mathrm{P},i} e_i(t) + \int_0^t K_{\mathrm{I},i} e_i(\tau)\, d\tau + \ldots \\ K_{\mathrm{D},i} \frac{de_i(t)}{dt} \frac{1}{T_{\mathrm{f},i} s + 1}, i \in \{1, 2\}. \tag{29}$$

3) INPUT TRANSFORMATION

The virtual control inputs $\boldsymbol{v}$ are obtained by combining the feedforward and feedback controllers:

$$\boldsymbol{v}(t) = \boldsymbol{v}_\mathrm{ff}(t) + \boldsymbol{v}_\mathrm{fb}(t). \tag{30}$$

However, since $\boldsymbol{v}$ cannot be directly applied to the system, the inverse input transformation (23) must be applied to obtain the actual inputs $\boldsymbol{u}$. Up until now, the physical limitations of the actuators, specifically the minimum and maximum compressor speeds of the cooling cycles, have not yet been considered. As a result, the input transformation could potentially violate these constraints. Rather than clipping the transformed control variables, which would compromise the decoupling achieved by the proposed control scheme, we present an alternative approach.

To minimize deviations between the virtual inputs $\boldsymbol{v}$ obtained from the control law in (30) and the virtual inputs that account for actuator constraints, $\boldsymbol{v}_\mathrm{con}$, we define the following quadratic cost function L:

$$\mathrm{L} = \frac{1}{2} [\boldsymbol{v}_\mathrm{con} - \boldsymbol{v}]^\mathrm{T} \boldsymbol{W} [\boldsymbol{v}_\mathrm{con} - \boldsymbol{v}], \tag{31}$$

where $\boldsymbol{W}$ is a diagonal weighting matrix. By applying the input transformation (22) to the constrained virtual

inputs, the optimal inputs $\boldsymbol{u}$ can be determined to minimize deviations from the desired inputs while satisfying the actuator constraints:

$$\begin{aligned}\boldsymbol{u} =& \arg\min_{\boldsymbol{u}} \frac{1}{2}\boldsymbol{u}^{\mathrm{T}}\boldsymbol{H}\boldsymbol{u} + \boldsymbol{F}^{\mathrm{T}}\boldsymbol{u} \\ & s.t.\ \boldsymbol{u}_{\min} \leq \boldsymbol{u} \leq \boldsymbol{u}_{\max}\end{aligned} \tag{32}$$

with

$$\begin{aligned}\boldsymbol{H} &= \boldsymbol{J}(\boldsymbol{x},\boldsymbol{d})^{\mathrm{T}}\boldsymbol{W}\boldsymbol{J}(\boldsymbol{x},\boldsymbol{d}) \\ \boldsymbol{F}^{\mathrm{T}} &= \boldsymbol{l}(\boldsymbol{x},\boldsymbol{d})^{\mathrm{T}}\boldsymbol{W}\boldsymbol{J}(\boldsymbol{x},\boldsymbol{d}) - \boldsymbol{v}^{\mathrm{T}}\boldsymbol{W}\boldsymbol{J}(\boldsymbol{x},\boldsymbol{d}),\end{aligned} \tag{33}$$

where $\boldsymbol{u}_{\min}$ and $\boldsymbol{u}_{\max}$ correspond to the minimum and maximum compressor speeds, respectively.

The weighting matrix $\boldsymbol{W}$ allows prioritization of minimal deviations from a specific desired virtual input $\boldsymbol{v}$, thereby prioritizing tracking one compartment temperature over the other when actuator constraints are active. When input constraints are inactive, the optimal inputs $\boldsymbol{u}$ correspond to the input transformation in (23) applied to the control law in (30).

D. PI CONTROLLER

For comparison with the proposed control scheme, a simple PI controller is used. Hence, both controllers have a similar feedback structure and complexity, as they both employ a PI/PID controller for feedback. The PI controller is adopted from the one used in the vapor compression cooling cycle of the test bed, which is described in the next section. This cooling cycle, along with its respective controller, is commercially used in the industry and thus represents an industry standard.

However, since PI controllers are only applicable for single-input single-output (SISO) control loops, i.e., loops with one input and one output, two separate control loops are designed, each assigning one input to a corresponding output. A logical choice is to have the compressor of cooling cycle 1 control the temperature inside the MT compartment, while the compressor speed of cooling cycle 2 controls the temperature of the LT compartment. Therefore, the control law of both PI controllers is given by:

$$u_{\mathrm{PI},i}(t) = K_{\mathrm{P},i}^{\mathrm{PI}} e_i(t) + \int_0^t K_{\mathrm{I},i}^{\mathrm{PI}} e_i(t)\, dt, \quad i \in \{1,2\} \tag{34}$$

with the controller parameters $K_{\mathrm{P},i}^{\mathrm{PI}}$ and $K_{\mathrm{I},i}^{\mathrm{PI}}$.

IV. EXPERIMENTAL EVALUATION

This section presents the experimental evaluation of the proposed multi-temperature transport system and its control scheme.

A. EXPERIMENTAL SETUP

Following the system architecture proposed in Section II, a test bed of the system is built (see Fig. 3), with its components specified in Table 1. The setup includes two commercially available vapor compression cooling cycles [49], intended for single-temperature applications.

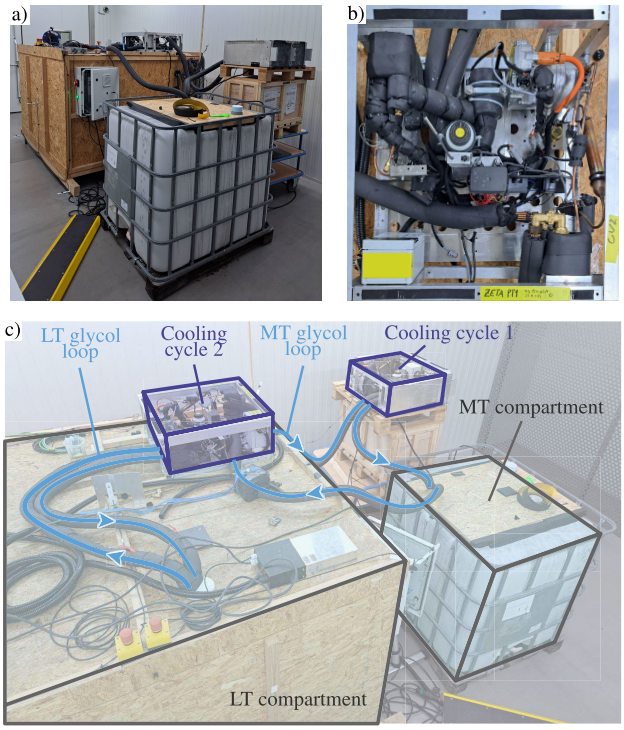

FIGURE 3. Overall view of the test bed (a), detailed view of cooling cycle 2 (b), and a top-down view of the test bed with its key components highlighted and labeled (c).

To accommodate the system architecture, the condenser of cooling cycle 2 is modified from a refrigerant-to-gas to a refrigerant-to-liquid configuration, and glycol loops are added. For the LT compartment, an insulated wooden box is used, while the MT compartment utilizes a smaller plastic container with less insulation. Although insulation and size of the compartments may vary in transport applications, this test bed effectively captures the overall system dynamics. Each compartment contains an electric heater to impose disturbance heat flows. All components are placed inside a climate chamber, enabling experiments under different ambient conditions.

The test bed's software is developed in MATLAB/Simulink [53] and executed on a dSPACE MicroLabBox [51], which interfaces with the system's sensors and controls its actuators. To implement the proposed continuous-time control system on the hardware, it is discretized using a fixed sampling time T_{s} during C-code generation for the MicroLabBox [54]. Since the sampling time is chosen significantly faster than the system dynamics, the effects of discretization are negligible. A PC manages the experiment and records the measurement data. The schematic illustrating the data processing and acquisition workflow is shown in Fig. 4.

B. CONTROLLER PARAMETRIZATION

Based on a training dataset acquired from open-loop experiments, the parameters of the control-oriented model

TABLE 1. Test bed specifications.

Component	Details
MT compartment:	
Description	Intermediate bulk container (IBC) [50]
Inner dimensions	120 cm x 100 cm x 115 cm
Volume	1000 L
LT compartment:	
Description	Self-build insulated box
Inner dimensions	120 cm x 160 cm x 180 cm
Volume	3456 L
Cooling cycle 1:	
Type	ecos M24 [49]
Refrigerant	R290 (propane)
Refrigerant charge	140g
Cooling cycle 2:	
Type	ecos M24 [49] (with condenser for refrigerant-to-liquid setup)
Refrigerant	R290 (propane)
Refrigerant charge	147g
Glycol loops:	
Fluid	Ethylene glycol water solution (35 vol%)
Data Acquisition:	
Real-time system	MicroLabBox [51]
Sampling time T_s	0.1s
Temperature measurements:	
Sensors	Dallas DS18S20 [52]
Accuracy	± 0.5°C

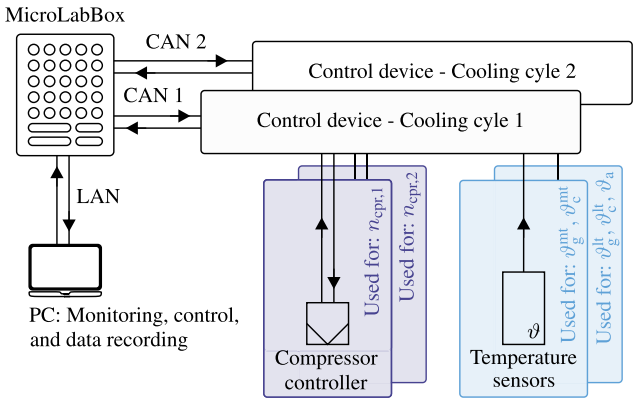

FIGURE 4. Schematic of the data acquisition and processing system for the test bed. The MicroLabBox communicates with the system components via a local area network (LAN) and two controller area networks (CAN).

are estimated using the method described in Section III-A. A validation experiment, shown in Fig. 5, confirms the accuracy of the model with the estimated parameters. During this validation experiment, the disturbances acting on the system $\boldsymbol{d}$ are held constant at $\boldsymbol{d} = [26°\text{C}, 0\text{W}, 1000\text{W}]$. The model's fit to the measurements (in percentage) for each state $x_i,\ i \in \{1, 2, 3, 4\}$ is quantified based on the normalized root mean squared error (NRMSE), as defined in [55]:

$$\text{Fit}_i = \left[1 - \sqrt{\frac{\sum_{k=1}^{n_k} \Delta x_i(t_k)^2}{\sum_{k=1}^{n_k} [x_{\text{meas},i}(t_k) - \bar{x}_{\text{meas},i}(t_k)]^2}}\right] \times 100\%, \tag{35}$$

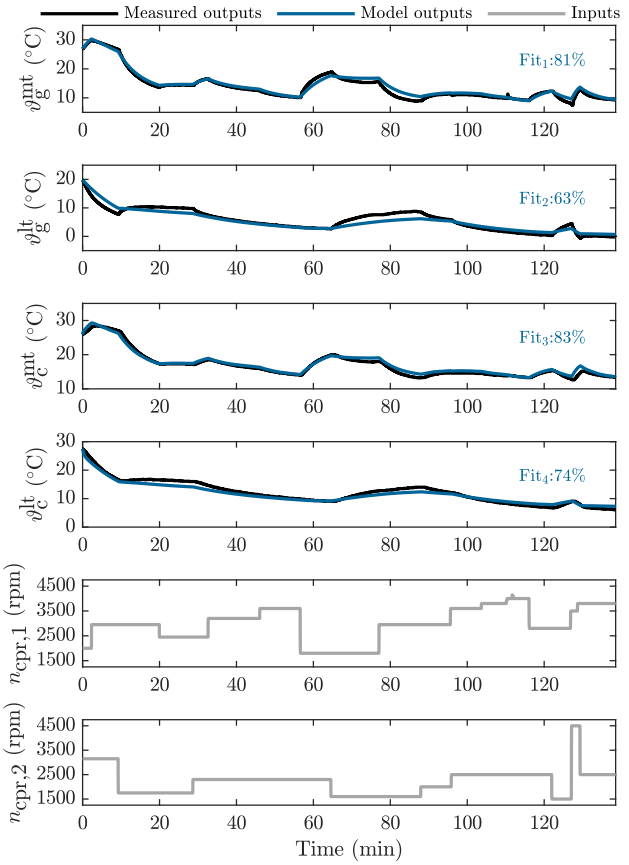

FIGURE 5. Validation experiment with prescribed inputs and comparison of measured states and model states. The model's fit to the measurement data is shown for each state.

where $\bar{x}_{\text{meas}}$ represents the arithmetic mean of the measured states. The numerical values of the estimated parameters $\boldsymbol{\theta}$ are given in the Appendix B.

Table 2 lists the parameters of the 2DOF controller. For trajectory planning, identical parameters are used for both outputs, ensuring no overshoot and a time constant compatible with the actuator limitations and the relatively slow dynamics of the thermal system. Although faster trajectory tuning would be possible, it could lead to frequent actuator saturation during operation, making it infeasible to follow the desired trajectory and thereby compromising control performance. Using the MATLAB PID tuner [56], the feedback controller is tuned for a faster response in the MT compartment. This approach was chosen because an aggressive LT controller would amplify interference more significantly than an aggressive MT controller in the case of imperfectly decoupled dynamics. For the optimization-based input transformation, two approaches are considered for the weighting matrix $\boldsymbol{W}$: one with higher weights on deviations from the MT compartment temperature trajectory ($\boldsymbol{W}_{\text{mt}}$), and one with higher weights on deviations from the LT compartment temperature trajectory ($\boldsymbol{W}_{\text{lt}}$). This results in two different controllers, denoted as 2DOF_{mt} with $\boldsymbol{W}_{\text{mt}}$ and

TABLE 2. Parameter values of the 2DOF controller.

Parameter	Value	Unit
Trajectory planning:		
τ_1, τ_2	200	s
λ_1, λ_2	1	-
Feedback control:		
$K_{\mathrm{P},1}$	$2.5 \cdot 10^{-3}$	s^{-2}
$K_{\mathrm{I},1}$	$9 \cdot 10^{-6}$	s^{-3}
$K_{\mathrm{D},1}$	0.05	s^{-1}
$T_{\mathrm{f},1}$	35	s
$K_{\mathrm{P},2}$	$4 \cdot 10^{-4}$	s^{-2}
$K_{\mathrm{I},2}$	$6 \cdot 10^{-7}$	s^{-3}
$K_{\mathrm{D},2}$	0.02	s^{-1}
$T_{\mathrm{f},2}$	90	s
Input transformation:		
$\boldsymbol{u}_{\min}$	1500	rpm
$\boldsymbol{u}_{\max}$	4500	rpm
$\boldsymbol{W}_{\mathrm{mt}}$	$\mathrm{diag}([10^{10}, 10^{8}])$	-
$\boldsymbol{W}_{\mathrm{lt}}$	$\mathrm{diag}([10^{8}, 10^{10}])$	-
Solver	quadprog [57]	-

$2\mathrm{DOF}_{\mathrm{lt}}$ with $\boldsymbol{W}_{\mathrm{lt}}$, which only differ when actuator constraints are active by prioritizing the tracking of one compartment temperature over the other.

The parameters of the PI controller used for comparison are adopted from the one integrated into the test bed's vapor compression cooling cycle, with $K_{\mathrm{P},i}^{\mathrm{PI}} = -700$ and $K_{\mathrm{I},i}^{\mathrm{PI}} = -4$ for both control loops $i \in \{1, 2\}$.

C. CONTROLLER RESULTS

Two experiments are conducted under different ambient conditions to evaluate the controllers: one at 15°C and the other at 25°C. During the experiment, random reference steps for the compartment temperatures are imposed. Care was taken to ensure that the experiments start under equivalent temperature conditions for each controller. The desired trajectories are initialized by applying the transformation (21) to the measured state vector and disturbances at the start. Due to the good insulation of the LT compartment and the requirement that temperatures should not fall far below the freezing point - since the test bed was not designed for such conditions - a 1000 W heating load is permanently active in the LT compartment using the electric heater. This heat load, along with ambient temperature measurements, is included in the disturbance vector $\boldsymbol{d}$ considered by the control law. The experimental results are presented in Fig. 6.

Figures 6a, b show the most important measured quantities of the two experiments over time. The results of the 2DOF controller, tuned for accurate temperature tracking of the MT compartment, are shown in purple, while the configuration prioritizing the LT compartment is depicted in green. The results of the PI controller are represented in gold. During the second experiment (Fig. 6b), external disturbances are introduced via the electric heaters inside the compartments. These disturbances, which were not included in the disturbance vector $\boldsymbol{d}$ and are therefore unknown to the controllers, are highlighted by orange markers, indicating both their duration and amplitude. For most of the experiments, both compartments are net cooled below ambient temperature. However, during experiment 1 (Fig. 6a), the MT compartment is heated above ambient temperature for certain periods.

Figure 6c shows two sections of the first experiment in detail, highlighting the system's response to reference steps for the two compartment temperatures. For the displayed time periods, the root mean squared errors (RMSE) are provided, calculated as

$$\mathrm{RMSE_i} = \sqrt{\frac{\sum_{k=1}^{n_\mathrm{k}} [y_{\mathrm{meas},i}(t_k) - y_{\mathrm{d},i}(t_k)]^2}{n_k}}, \quad i \in \{1, 2\}, \tag{36}$$

where the samples t_k, $k \in \{1, \ldots, n_\mathrm{k}\}$ are taken from the shown periods.

Furthermore, Fig. 6d presents the RMSE values for both experiments, where the time series data has been divided into seven intervals $\mathcal{I}_i$, $i \in \{1, 2, \ldots, 7\}$ to allow for a more detailed analysis. These intervals, highlighted in Fig. 6a,b, are grouped into two categories: those where control actions are significantly restricted by actuator constraints (shown on the right of Fig. 6d and marked with *), and those where they are not (shown on the left). The average RMSE for the intervals largely unaffected by actuator constraints is provided, while computing the average for the other intervals is not sensible due to the large variations in RMSE values.

1) REGULAR INTERVALS

In intervals not significantly impacted by actuator limits, the controllers generally perform well in tracking the reference values. The two 2DOF controllers perform similarly in these intervals, as their control laws are identical when no actuator constraints are active. However, notable differences are evident when comparing them to the PI controller, which shows substantial tracking errors, as seen in both the time-series data and RMSE values. The RMSE values remain relatively consistent across intervals $\mathcal{I}_2$, $\mathcal{I}_3$, and $\mathcal{I}_4$, except for $\mathcal{I}_7$, where larger deviations occur due to unknown disturbances introduced in this interval. Despite this, all controllers manage to compensate for the unknown disturbances. On average, across these four intervals, the proposed 2DOF controllers significantly reduce temperature deviations compared to the PI controller, achieving RMSE reductions between 40% and 77%.

The advantage of the 2DOF controllers stems from their decoupling control law, as particularly evident in Fig. 6c. For the 2DOF controller, a reference change in either the MT or LT compartment affects only the corresponding compartment temperature, while the other remains largely unaffected. In contrast, the PI controller does not account for the system's coupled dynamics, leading to significant deviations from the desired compartment temperatures. This effect is especially noticeable for the reference step of the LT compartment, as the inherent coupling causes considerable temperature deviations from the desired trajectory in the MT

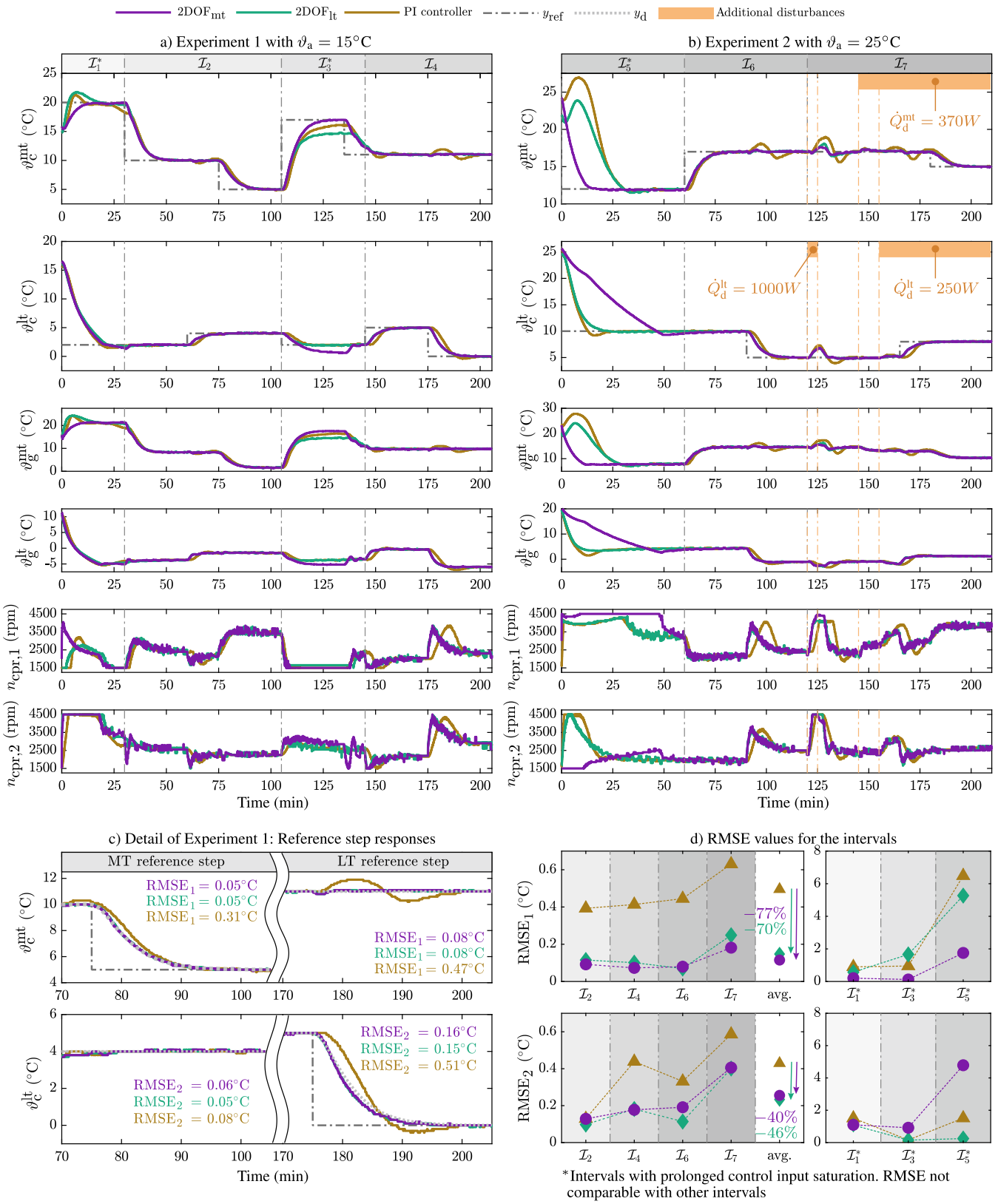

FIGURE 6. Experimental results of the three controllers, showing the full time-domain data in (a) and (b), a detailed view of selected periods from Experiment 1 highlighting reference steps for the MT and LT compartments in (c), and the RMSE values for the intervals $\mathcal{I}_i$, $i \in \{1, 2, \ldots, 7\}$ in (d).

compartment. For the reference step of the MT compartment temperature, the coupling effects are less pronounced due to the chosen input-output assignment of the PI controller. The benefits of the proposed controller are further demonstrated in the time series data shown in Fig. 6b, particularly during the period when unknown disturbances affect the system, leading to an inaccurate model being used by the 2DOF controllers. Upon the onset of the disturbance, both compartment temperatures deviate from their references. Although perfect decoupling is not achieved, the 2DOF controller is still able to partially decouple the system, even with the imperfect model. Consequently, the 2DOF controller significantly outperforms the PI controller immediately after the disturbances affect the system. Furthermore, during intervals with active unknown disturbances, the 2DOF controller accurately tracks the reference trajectories, including step changes in the reference temperatures of both compartments, without noticeable coupling effects, demonstrating the robustness of the proposed control approach.

2) INTERVALS DOMINATED BY ACTUATOR CONSTRAINTS

During intervals when actuator constraints are active for extended durations, temperature tracking performance varies significantly between controllers. These constraints become active due to rapid temperature changes required by the desired trajectory during initial cooldown ($\mathcal{I}_1$ and $\mathcal{I}_5$) or by an infeasible combination of reference temperatures given the actuator limits ($\mathcal{I}_3$). During these intervals, the differences between the two 2DOF controllers are apparent due to the different prioritization in the input transformation. During initial cooldown, the prioritized compartment reaches its reference temperature faster for both 2DOF controllers, and in cases of infeasible reference temperatures, only the prioritized compartment temperature is tracked in steady state. This distinction is further reflected in the RMSE values for both 2DOF configurations, with the RMSE for the prioritized compartment being significantly lower than for the non-prioritized one. In the intervals dominated by actuator constraints, the PI controller performs similarly to the $2DOF_{lt}$ controller.

During interval $\mathcal{I}_3$ of experiment 1, the subordinate compressor speed controller malfunctioned with the $2DOF_{lt}$ controller, preventing the speed from reaching the minimum of 1500 rpm. As a result, the speed remained slightly higher at 1550 rpm, which explains the differences in MT compartment temperature between the PI and $2DOF_{lt}$ controller during this interval. Furthermore, in experiment 2, the refrigeration system's power supply reached its power limit at times with both the $2DOF_{lt}$ and PI controller. This is evident in interval $\mathcal{I}_5$ and, for a short period, in $\mathcal{I}_7$, where the power limit prevented the compressor from reaching its maximum speed despite being prescribed by both controllers. This issue was resolved for the remainder of the experiments.

V. DISCUSSION

The proposed multi-temperature refrigeration system significantly reduces refrigerant charge compared to conventional systems with similar cooling capacity [58], [59], [60]. This reduction is achieved through an indirect architecture utilizing glycol cycles, enabling a compact cooling cycle design. Furthermore, this compact design offers two key advantages: first, it facilitates hermetic sealing of the cooling cycle, effectively preventing refrigerant leakage. Second, it simplifies assembly and maintenance due to the absence of refrigerant lines distributed to the compartments. As a result, the cooling cycle can be preassembled in the factory rather than during the assembly of the transport system, such as in a refrigerated vehicle. This not only enhances safety - particularly given the use of propane as a refrigerant - but also reduces installation costs by eliminating the need for a thermal technician during final assembly.

Furthermore, the proposed architecture enables efficient heating of the MT compartment, which may be necessary at low ambient temperatures. Conventional systems typically rely on electric heaters inside the heat exchanger, which are inefficient. In contrast, the proposed design utilizes waste heat from cooling cycle 2 to heat the MT compartment. Additionally, this heating mode can be used for defrosting the heat exchanger, which is a major challenge in refrigerated transport systems, as defrosting accounts for a significant portion of their total energy consumption [61], [62].

While the test bed may differ from real-world refrigerated transport systems in size, insulation, and housing, the results confirm the system's feasibility. Although some time constants may vary, the overall system dynamics are well captured, allowing insights into system performance and effective evaluation of the control scheme. For deployment in applications of different scales, model and controller parameters would need to be adapted to the specific target system. Nonetheless, the underlying control structure and methodology are inherently scalable and remain transferable to systems of different sizes.

Furthermore, the proposed 2DOF control concept demonstrates excellent performance and effectively decouples the output dynamics through feedback linearization, as experimentally validated on the test bed. As a result, the desired compartment temperatures are accurately tracked and temperature deviations in the compartments are significantly reduced compared to a non-decoupling control concept.

An additional advantage of the control scheme is its ease of tuning. First, unlike other multivariable control approaches, the proposed scheme can be tuned using SISO control loops due to the decoupling achieved via feedback linearization. This is generally preferred, as tuning SISO loops is considerably simpler than tuning a multi-input-multi-output (MIMO) system with multiple inputs and outputs [63]. Second, the 2DOF control structure allows for independent tuning of the response to reference temperature changes and disturbance rejection. For example, if goods require a slow cooldown from ambient temperature to prevent thermal shock - which could potentially damage them

- the control scheme can accommodate this requirement while still maintaining an aggressive disturbance rejection strategy. Third, the control law can be adjusted to prioritize temperature tracking in one compartment over another or to maintain equal priority between compartments. This flexibility enables customization of the control strategy based on specific application needs.

One limitation of the proposed 2DOF controller is its dependence on an accurate system model, unlike model-free approaches such as the PI controller used for comparison. While the model used in this work is relatively simple, it captures the essential system dynamics and has proven sufficiently accurate to ensure good control performance. At the same time, it maintains low computational complexity and allows for straightforward parameterization, requiring only limited experimental measurement data. Although more detailed models of vapor compression cycles [64], compartment walls [42], and specific exogenous disturbances such as solar radiation [65] or compartment door openings [66] are available, the proposed framework allows for their straightforward integration if higher modeling accuracy is required.

Furthermore, the control strategy itself is deliberately kept simple, employing a basic 2DOF structure with straightforward trajectory planning and PID-based feedback control. This results in a minimal computational load, enabling real-time implementation on the test bed and demonstrating the feasibility of the approach for deployment in real-world multi-temperature transport systems. In contrast, more advanced strategies such as trajectory planning methods that account for actuator constraints or energy consumption [67], [68], and MPC schemes that anticipate future system behavior [69], [70], typically demand significantly higher computational resources. Nonetheless, if more sophisticated methods are required, they can be integrated into the proposed control framework based on the feedback-linearized system developed in this study.

Future extensions of this work could involve integrating the system's energy consumption into the control law, thus transforming the problem into a multi-objective one. In this context, trajectory planning should aim not only to reach the desired compartment reference temperatures with specified dynamic behavior, but also to minimize energy consumption during the transition. This multi-objective problem could be addressed using optimization techniques, such as dynamic programming [71]. Furthermore, incorporating the ability to deactivate cooling cycles and adjust fan and pump speeds could broaden the system's operating range, thereby enhancing the flexibility of the control scheme - an aspect that should be investigated in future research.

VI. CONCLUSION

This work presents a novel refrigeration system and control strategy designed to enhance efficiency, reliability, and sustainability in multi-temperature transport systems. The proposed indirect refrigeration system, utilizing glycol loops for each compartment, enables a compact cooling cycle design, significantly reducing refrigerant charge and leakage potential and thereby minimizing the environmental impact of refrigerant emissions.

By applying feedback linearization to a nonlinear model of the refrigeration system, a 2DOF controller is designed to eliminate the coupled dynamics of the compartment temperatures in the closed loop. The control scheme includes a trajectory planning algorithm and a feedback controller to mitigate tracking errors. Actuator constraints are directly considered in the control scheme, allowing the prioritization of one compartment's temperature control when accurate tracking of both is not feasible.

Experimental evaluation of the 2DOF controller on a dedicated test bed demonstrates that deviations in compartment temperatures can be significantly reduced by mitigating the system's coupled dynamics. Specifically, during normal operation - where reference steps in compartment temperatures were imposed and the system was subjected to unknown disturbances - temperature deviations were reduced by 40% to 77% compared to a conventional PI controller. Consequently, the risk of damage or loss of goods due to inadequate temperature conditions during transport is minimized. Ultimately, the proposed refrigeration system and control strategy enhance sustainability and reduce the environmental impact of multi-temperature transport systems.

APPENDIX

A. ABBREVIATIONS

The following abbreviations are used in this manuscript:

2DOF	Two-degree-of-freedom.
CAN	Controller area network.
DX	Direct expansion.
GWP	Global warming potential.
HFC	Hydrofluorocarbon.
IDX	Indirect expansion.
LAN	Local area network.
LT	Low temperature.
MIMO	Multi-input-multi-output.
MPC	Model predictive controller.
MT	Medium temperature.
NRMSE	Normalized root mean squared error.
PID	Proportional–integral–derivative.
RMSE	Root mean squared error.
SISO	Single-input single-output

B. PARAMETER VALUES

The estimated model parameter values obtained from experimental data are presented in Table 3.

TABLE 3. Model parameter values.

Parameter	Value	Unit
C_c^{mt}	$1.20 \cdot 10^3$	J K^{-1}
C_c^{lt}	$4.20 \cdot 10^3$	J K^{-1}
C_g^{mt}	$8.75 \cdot 10^4$	J K^{-1}
C_g^{lt}	$8.46 \cdot 10^4$	J K^{-1}
K_c^{mt}	185	W K^{-1}
K_c^{lt}	198	W K^{-1}
K_w^{mt}	59.8	W K^{-1}
K_w^{lt}	16.0	W K^{-1}
$\alpha_{1,1}$	-0.0298	W K^{-1} rpm^{-1}
$\alpha_{2,1}$	0.0552	W K^{-1} rpm^{-1}
$\alpha_{3,1}$	-5.32	W rpm^{-1}
$\alpha_{1,2}$	-0.00636	W K^{-1} rpm^{-1}
$\alpha_{2,2}$	0.0320	W K^{-1} rpm^{-1}
$\alpha_{3,2}$	-6.43	W rpm^{-1}
$\beta_{1,2}$	-0.0262	W K^{-1} rpm^{-1}
$\beta_{2,2}$	0.0639	W K^{-1} rpm^{-1}
$\beta_{3,2}$	-8.44	W rpm^{-1}

C. NONSINGULAR COUPLING MATRIX

By applying the method described in Section III-B, the coupling matrix is computed as

$$\boldsymbol{J}(\boldsymbol{x},\boldsymbol{d}) = \begin{bmatrix} \frac{-K_c^{mt}(\alpha_{1,1}T_a+\alpha_{2,1}T_g^{mt}+\alpha_{3,1})}{C_g^{mt}C_c^{mt}} & \frac{K_c^{mt}(\beta_{1,2}T_g^{mt}+\beta_{2,2}T_g^{lt}+\beta_{3,2})}{C_g^{mt}C_c^{mt}} \\ 0 & \frac{-K_c^{lt}(\alpha_{1,2}T_g^{mt}+\alpha_{2,2}T_g^{lt}+\alpha_{3,2})}{C_g^{lt}C_c^{lt}} \end{bmatrix}. \tag{37}$$

To determine when the coupling matrix $\boldsymbol{J}$ is singular, its variables T_g^{mt}, T_g^{lt}, and T_a are bounded within a physically reasonable range between -10°C and 30°C. To check for singularities, the determinant of the coupling matrix is computed and set to zero, i.e.,

$$\det \boldsymbol{J}(\boldsymbol{x},\boldsymbol{d}) = 0. \tag{38}$$

Inserting the parameter values given in Table 3, yields the following linear problem:

$$\begin{aligned} 15.9\, T_g^{mt} - 8.58\, T_a &= 1530 \\ -3.7\, T_g^{mt} + 18\, T_g^{lt} &= 3700 \\ s.t\ \ 263.15\ \text{K} \le T_g^{mt}, T_g^{lt}, T_a &\le 303.15\ \text{K}. \end{aligned} \tag{39}$$

Since this linear problem is infeasible, there is no combination of variables that satisfies the singularity condition (38). Therefore, the coupling matrix $\boldsymbol{J}$ remains nonsingular within the defined operating region, validating the assumption of a nonsingular coupling matrix for the system.

ACKNOWLEDGMENT

The authors gratefully acknowledge the support of PBX GmbH for their help with experimental investigations and data acquisition.

REFERENCES

[1] O. Adekomaya, T. Jamiru, R. Sadiku, and Z. Huan, "Sustaining the shelf life of fresh food in cold chain—A burden on the environment," *Alexandria Eng. J.*, vol. 55, no. 2, pp. 1359–1365, Jun. 2016.
[2] X. She, L. Cong, B. Nie, G. Leng, H. Peng, Y. Chen, X. Zhang, T. Wen, H. Yang, and Y. Luo, "Energy-efficient and -economic technologies for air conditioning with vapor compression refrigeration: A comprehensive review," *Appl. Energy*, vol. 232, pp. 157–186, Dec. 2018.
[3] S. Minetto, F. Fabris, S. Marinetti, and A. Rossetti, "A review on present and forthcoming opportunities with natural working fluids in transport refrigeration," *Int. J. Refrig.*, vol. 152, pp. 343–355, Aug. 2023.
[4] C. Francis, G. Maidment, and G. Davies, "An investigation of refrigerant leakage in commercial refrigeration," *Int. J. Refrig.*, vol. 74, pp. 12–21, Feb. 2017.
[5] A. Maiorino, F. Petruzziello, and C. Aprea, "Refrigerated transport: State of the art, technical issues, innovations and challenges for sustainability," *Energies*, vol. 14, no. 21, p. 7237, Nov. 2021.
[6] Y. Li, J. Yang, X. Wu, Y. Liu, Y. Zhuang, P. Zhou, X. Han, and G. Chen, "Leakage, diffusion and distribution characteristics of refrigerant in a limited space: A comprehensive review," *Thermal Sci. Eng. Prog.*, vol. 40, May 2023, Art. no. 101731.
[7] A. G. Kehinde, T. Ngonda, A. Raji, and K. Kanyarusoke, "A review of different technologies for refrigerated truck," *Mater. Today, Proc.*, vol. 56, pp. 2305–2310, Jan. 2022.
[8] M. Ostermeier, T. Henke, A. Hübner, and G. Wäscher, "Multi-compartment vehicle routing problems: State-of-the-art, modeling framework and future directions," *Eur. J. Oper. Res.*, vol. 292, no. 3, pp. 799–817, Aug. 2021.
[9] A. Hübner and M. Ostermeier, "A multi-compartment vehicle routing problem with loading and unloading costs," *Transp. Sci.*, vol. 53, no. 1, pp. 282–300, Feb. 2019.
[10] M. Frank, M. Ostermeier, A. Holzapfel, A. Hübner, and H. Kuhn, "Optimizing routing and delivery patterns with multi-compartment vehicles," *Eur. J. Oper. Res.*, vol. 293, no. 2, pp. 495–510, Sep. 2021.
[11] M. Ostermeier and A. Hübner, "Vehicle selection for a multi-compartment vehicle routing problem," *Eur. J. Oper. Res.*, vol. 269, no. 2, pp. 682–694, Sep. 2018.
[12] A. S. Gaur, D. Z. Fitiwi, and J. Curtis, "Heat pumps and our low-carbon future: A comprehensive review," *Energy Res. Social Sci.*, vol. 71, Jan. 2021, Art. no. 101764.
[13] K. Nawaz and M. R. Ally, "Options for low-global-warming-potential and natural refrigerants part 2: Performance of refrigerants and systemic irreversibilities," *Int. J. Refrig.*, vol. 106, pp. 213–224, Oct. 2019.
[14] V. Nair, "HFO refrigerants: A review of present status and future prospects," *Int. J. Refrig.*, vol. 122, pp. 156–170, Feb. 2021.
[15] E. A. Heath, "Amendment to the Montreal protocol on substances that deplete the ozone layer (Kigali Amendment)," *Int. Legal Mater.*, vol. 56, no. 1, pp. 193–205, Feb. 2017.
[16] R. B. Barta, E. A. Groll, and D. Ziviani, "Review of stationary and transport CO_2 refrigeration and air conditioning technologies," *Appl. Thermal Eng.*, vol. 185, Feb. 2021, Art. no. 116422.
[17] S. Elbel, M. Visek, and P. Hrnjak, "A fair comparison of CO_2 and propane used in light commercial applications featuring natural refrigerants," in *Proc. Int. Refrig. Air Conditioning Conf.*, Jul. 2016, pp. 1–9, Paper 1748. [Online]. Available: http://docs.lib.purdue.edu/iracc/1748
[18] F. Fabris, M. Fabrizio, S. Marinetti, A. Rossetti, and S. Minetto, "Evaluation of the carbon footprint of HFC and natural refrigerant transport refrigeration units from a life-cycle perspective," *Int. J. Refrig.*, vol. 159, pp. 17–27, Mar. 2024.
[19] D. Colbourne, P. Solomon, R. Wilson, L. De Swardt, R. Nosbers, and M. Schuster, "Development of R290 transport refrigeration system," in *Proc. IOR*, Mar. 2017, pp. 1–14. [Online]. Available: https://secure.toolkitfiles.co.uk/clients/33346/sitedata/files/MACP-News-Article-10.03.17-20170310141830.pdf
[20] M. Ramaube and Z. Huan, "Testing and performance evaluation of a R404A transport refrigeration system retrofitted with R290," in *Proc. AIUE 17th Ind. Commercial Use Energy (ICUE) Conf.*, Cape Town, South Africa, Nov. 2019, pp. 1–8. [Online]. Available: https://ssrn.com/abstract=3658977
[21] C. Arpagaus, F. Bless, J. Schiffmann, and S. S. Bertsch, "Multi-temperature heat pumps: A literature review," *Int. J. Refrig.*, vol. 69, pp. 437–465, Sep. 2016.
[22] S. Boahen and J. Choi, "Research trend of cascade heat pumps," *Sci. China Technol. Sci.*, vol. 60, no. 11, pp. 1597–1615, Nov. 2017.

[23] M. Pan, H. Zhao, D. Liang, Y. Zhu, Y. Liang, and G. Bao, "A review of the cascade refrigeration system," *Energies*, vol. 13, no. 9, p. 2254, May 2020.

[24] Y.-D. Zhu, Z.-R. Peng, G.-B. Wang, and X.-R. Zhang, "Thermodynamic analysis of a novel multi-target-temperature cascade cycle for refrigeration," *Energy Convers. Manage.*, vol. 243, Sep. 2021, Art. no. 114380.

[25] S. Smyth, D. Finn, and B. Brophy, "Performance evaluation of an economised indirect multi-temperature transport refrigeration system," in *Proc. Int. Refrig. Air Conditioning Conf.*, Dec. 2010, pp. 1–9, Art. no. 1095. [Online]. Available: https://docs.lib.purdue.edu/iracc/index.16.html#year_2010

[26] K. Wang, M. Eisele, Y. Hwang, and R. Radermacher, "Review of secondary loop refrigeration systems," *Int. J. Refrig.*, vol. 33, no. 2, pp. 212–234, Mar. 2010.

[27] Q. Liu, Z. Sun, Q. Wang, X. Bai, C. Su, Y. Liang, S. Tian, H. Sun, J. Peng, S. Liu, S. Dong, and K. Hu, "Influence of secondary fluid on the performance of indirect refrigeration system," *Appl. Thermal Eng.*, vol. 197, Oct. 2021, Art. no. 117388.

[28] D. Sánchez, R. Cabello, R. Llopis, J. Catalán-Gil, and L. Nebot-Andrés, "Energy assessment and environmental impact analysis of an R134a/R744 cascade refrigeration plant upgraded with the low-GWP refrigerants r152a, R1234ze(E), propane (R290) and propylene (R1270)," *Int. J. Refrig.*, vol. 104, pp. 321–334, Aug. 2019.

[29] R. Llopis, D. Sánchez, R. Cabello, J. Catalán-Gil, and L. Nebot-Andrés, "Conversion of a direct to an indirect refrigeration system at medium temperature using R-134a and R-507A: An energy impact analysis," *Appl. Sci.*, vol. 8, no. 2, p. 247, Feb. 2018.

[30] D. Sánchez, R. Llopis, R. Cabello, J. Catalán-Gil, and L. Nebot-Andrés, "Conversion of a direct to an indirect commercial (HFC134a/CO_2) cascade refrigeration system: Energy impact analysis," *Int. J. Refrig.*, vol. 73, pp. 183–199, Jan. 2017.

[31] R. Jedermann, U. Praeger, M. G. Leibniz, and W. Lang, "Temperature deviations during transport as a cause for food losses," in *Preventing Food Losses and Waste to Achieve Food Security and Sustainability*. Cambridge, U.K.: Burleigh Dodds Science Publishing, 2020, pp. 301–340.

[32] J. Koeln, B. Keating, A. Alleyne, C. Price, and B. P. Rasmussen, *Multi-Zone Temperature Modeling and Control*. Cham, Switzerland: Springer, 2018, pp. 139–166.

[33] D. J. Burns, C. Danielson, S. Di Cairano, C. R. Laughman, and S. A. Bortoff, *Model Predictive Control of Multi-Zone Vapor Compression Systems*. Cham, Switzerland: Springer International Publishing, 2018, pp. 105–137.

[34] J. P. Koeln and A. G. Alleyne, "Decentralized controller analysis and design for multi-evaporator vapor compression systems," in *Proc. Amer. Control Conf.*, Jun. 2013, pp. 437–442.

[35] M. Gräber, C. Kirches, J. P. Schlöder, and W. Tegethoff, "Nonlinear model predictive control of a vapor compression cycle based on first principle models," *IFAC Proc. Volumes*, vol. 45, no. 2, pp. 258–263, 2012.

[36] M. Elnour and N. Meskin, "Multi-zone HVAC control system design using feedback linearization," in *Proc. 5th Int. Conf. Control, Instrum., Autom. (ICCIA)*, Nov. 2017, pp. 249–254.

[37] A. Thosar, A. Patra, and S. Bhattacharyya, "Feedback linearization based control of a variable air volume air conditioning system for cooling applications," *ISA Trans.*, vol. 47, no. 3, pp. 339–349, Jul. 2008.

[38] L. Sun and F. You, "Machine learning and data-driven techniques for the control of smart power generation systems: An uncertainty handling perspective," *Engineering*, vol. 7, no. 9, pp. 1239–1247, Sep. 2021.

[39] W. Wang, Y. Li, and B. Hu, "Real-time efficiency optimization of a cascade heat pump system via multivariable extremum seeking," *Appl. Thermal Eng.*, vol. 176, Jul. 2020, Art. no. 115399.

[40] Y. Li, X. Pan, X. Liao, and Z. Xing, "A data-driven energy management strategy based on performance prediction for cascade refrigeration systems," *Int. J. Refrig.*, vol. 136, pp. 114–123, Apr. 2022.

[41] F. Fabris, P. Artuso, S. Marinetti, S. Minetto, and A. Rossetti, "Cooling unit impact on energy and emissions of a refrigerated light truck," *Appl. Thermal Eng.*, vol. 216, Nov. 2022, Art. no. 119132.

[42] M. Fallmann, A. Poks, and M. Kozek, "Control-oriented hybrid model of a small-scale refrigerated truck chamber," *Appl. Thermal Eng.*, vol. 220, Feb. 2023, Art. no. 119719.

[43] J. P. Holman, *Heat Transfer* (McGraw-Hill Series in Mechanical Engineering), 10th ed., Boston, MA, USA: McGraw-Hill, 2010.

[44] E. Luchini, A. Poks, D. Radler, and M. Kozek, "Model predictive temperature control for a food transporter with door-openings," in *Proc. SICE Int. Symp. Control Syst. (SICE ISCS)*, Mar. 2020, pp. 85–91.

[45] A. Isidori, *Nonlinear Control Systems* (Communications and Control Engineering), 3rd ed., London, U.K.: Springer, 2000.

[46] H. K. Khalil, *Nonlinear Systems* (Always Learning), 3rd ed., Harlow, U.K.: Pearson, 2014.

[47] V. Hagenmeyer and E. Delaleau, "Robustness analysis of exact feedforward linearization based on differential flatness," *Automatica*, vol. 39, no. 11, pp. 1941–1946, Nov. 2003.

[48] I. D. Díaz-Rodríguez, S. Han, and S. P. Bhattacharyya, *Analytical Design of PID Controllers*. Cham, Switzerland: Springer, 2019.

[49] PBX GmbH. (2025). *ECOS M24*. Accessed: Jan. 29, 2025. [Online]. Available: https://pbx.at/solutions/

[50] *Intermediate Bulk Containers (IBCs) for Non-Dangerous Goods*, ISO Standard 15867:2003, Geneva, Switzerland, 2003.

[51] dSPACE GmbH. (2025). *Microlabbox*. Accessed: Jan. 29, 2025. [Online]. Available: https://www.dspace.com/en/pub/home/products/hw/microlabbox.cfm

[52] Analog Devices Inc. (2025). *Ds18s20*. Accessed: Feb. 25, 2025. [Online]. Available: https://www.analog.com/en/products/ds18s20.html

[53] The MathWorks Inc. *MATLAB Version: 9.9.0 (R2020b)*. Accessed: Feb. 2, 2024. [Online]. Available: https://www.mathworks.com

[54] dSPACE GmbH. (2025). *Real-Time Interface*. Accessed: Feb. 10, 2025. [Online]. Available: https://www.dspace.com/de/gmb/home/products/sw/impsw/real-time-interface.cfm

[55] The MathWorks Inc. *System Identification Toolbox*. Accessed: Feb. 10, 2024. [Online]. Available: https://mathworks.com/help/ident/ref/compare.html

[56] The MathWorks Inc. *MATLAB PID Tuner*. Accessed: Feb. 18, 2024. [Online]. Available: https://mathworks.com/help/control/ref/pidtuner-app.html

[57] The MathWorks Inc. *Optimization Toolbox Version: 9.0 (R2020b)*. Accessed: Feb. 2, 2024. [Online]. Available: https://www.mathworks.com

[58] Thermo King Europe. (2023). *Vx-Series*. Accessed: Feb. 13, 2025. [Online]. Available: https://thermokingzapp.com/assets/original/TK80083_Vx-Series_02-2023_EN_V2.0_LRpp.pdf

[59] Monzone Air-conditioning Pte Ltd. (2025). *V Series for Large or Medium Vehicles*. Accessed: Feb. 13, 2025. [Online]. Available: http://www.monzone-aircon.com/products-category.asp?cat=11

[60] F. Poggi, H. Macchi-Tejeda, D. Leducq, and A. Bontemps, "Refrigerant charge in refrigerating systems and strategies of charge reduction," *Int. J. Refrigeration*, vol. 31, no. 3, pp. 353–370, May 2008.

[61] K. Nawaz, A. F. Elatar, and B. A. Fricke, "A critical literature review of defrost technologies for heat pumps and refrigeration systems," Oak Ridge Nat. Lab. (ORNL), Oak Ridge, TN, USA, Tech. Rep. ORNL/SPR-2018/1007. [Online]. Available: https://www.osti.gov/biblio/1474464

[62] M. Amer and C.-C. Wang, "Review of defrosting methods," *Renew. Sustain. Energy Rev.*, vol. 73, pp. 53–74, Jun. 2017.

[63] N. Jain, R. J. Otten, and A. G. Alleyne, "Decoupled feedforward control for an air-conditioning and refrigeration system," in *Proc. Amer. Control Conf.*, Jun. 2010, pp. 5904–5909.

[64] B. P. Rasmussen, C. Price, J. Koeln, B. Keating, and A. Alleyne, *HVAC System Modeling and Control: Vapor Compression System Modeling and Control*. Cham, Switzerland: Springer, 2018, pp. 73–103.

[65] A. Maiorino, A. Mota-Babiloni, F. Petruzziello, M. G. Del Duca, A. Ariano, and C. Aprea, "A comprehensive energy model for an optimal design of a hybrid refrigerated van," *Energies*, vol. 15, no. 13, p. 4864, Jul. 2022.

[66] T. Lafaye de Micheaux, M. Ducoulombier, J. Moureh, V. Sartre, and J. Bonjour, "Experimental and numerical investigation of the infiltration heat load during the opening of a refrigerated truck body," *Int. J. Refrig.*, vol. 54, pp. 170–189, Jun. 2015.

[67] Y. Taniai, T. Naniwa, and J. Nishii, "Optimal reaching trajectories based on feedforward control," *Biol. Cybern.*, vol. 116, no. 4, pp. 517–526, Aug. 2022.

[68] A. Poks, A. Schirrer, and M. Kozek, "Energy management in refrigerated electric small transport: A hierarchical approach," *IEEE Access*, vol. 12, pp. 183918–183936, 2024.

[69] M. Fallmann, M. Lösch, A. Poks, and M. Kozek, "Energy-efficient hybrid model predictive control of mobile refrigeration systems," *Appl. Thermal Eng.*, vol. 235, Nov. 2023, Art. no. 121347.

[70] S. E. Shafiei and A. Alleyne, "Model predictive control of hybrid thermal energy systems in transport refrigeration," *Appl. Thermal Eng.*, vol. 82, pp. 264–280, May 2015.

[71] R. Bellman and S. Dreyfus, *Dynamic Programming*, vol. 33. Princeton, NJ, USA: Princeton Univ. Press, 2010. [Online]. Available: http://www.jstor.org/stable/j.ctv1nxcw0f

MAXIMILIAN LÖSCH received the M.Sc. degree in mechanical engineering from TU Wien, Vienna, Austria, in 2022.

Since 2022, he has been a Project Assistant with the Institute of Mechanics and Mechatronics, TU Wien. His current research interests include the modeling of thermal systems, nonlinear control systems, and optimization.

STEFAN JAKUBEK received the M.S. degree in mechanical engineering, the Ph.D. degree in technical sciences, and the Habilitation (professorial qualification) degree in control theory and system dynamics from TU Wien, Vienna, Austria, in 1997, 2000, and 2007, respectively.

From 2006 to 2009, he was the Head of Development for Hybrid Powertrain Calibration and Battery Testing Technology, Automotive Industry Company, AVL List GmbH, Graz, Austria. He is currently a Professor and the Head of the Institute of Mechanics and Mechatronics, TU Wien. His research interests include fault diagnosis, nonlinear system identification, and simulation technology.

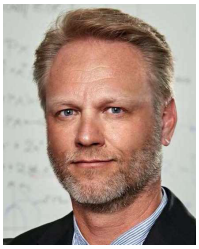

MARTIN KOZEK received the M.S. degree in mechanical engineering and the Ph.D. and Habilitation degrees from TU Wien, Vienna, Austria, in 1994, 2000, and 2009, respectively. He is currently a Professor with the Institute of Mechanics and Mechatronics, TU Wien. His research interests include nonlinear systems modeling and identification, model predictive process control, and active control of structural vibrations.